

Embedding dynamical mean-field theory for superconductivity in layered materials and heterostructures

Francesco Petocchi and Massimo Capone

International School for Advanced Studies (SISSA/ISAS) and CNR-IOM Democritos, Via Bonomea 265, 34136, Trieste, Italy

(Received 13 January 2016; revised manuscript received 15 May 2016; published 15 June 2016)

We study layered systems and heterostructures of s -wave superconductors by means of a suitable generalization of dynamical mean-field theory. In order to reduce the computational effort, we consider an embedding scheme in which a relatively small number of active layers is embedded in an effective potential accounting for the effect of the rest of the system. We introduce a feedback of the active layers on the embedding potential that improves on previous approaches and essentially eliminates the effects of the finiteness of the active slab allowing for cheap computation of very large systems. We extend the method to the superconducting state, and we benchmark the approach by means of simple paradigmatic examples showing some examples on how an interface affects the superconducting properties. As examples, we show that superconductivity can penetrate from an intermediate coupling superconductor into a weaker coupling one for around ten layers, and that the first two layers of a system with repulsive interaction can turn superconducting by proximity effects even when charge redistribution is inhibited.

DOI: [10.1103/PhysRevB.93.235125](https://doi.org/10.1103/PhysRevB.93.235125)

I. INTRODUCTION

The advances in manufacturing and handling heterostructures are in the forefront of solid state research. In particular, heterostructure based on oxides have a huge potential thanks to the rich physics of their constituents. Combining different oxides one can even engineer and tailor electronic and magnetic states which can be completely different from those of the bulk constituents. The possibility to control these emergent and intrinsic properties of the constituents opens an avenue towards the realization of new devices based on correlated electrons.

One of the most studied examples of the novel physics at oxide interfaces is the appearance of a high-mobility electron gas at the interface between the band insulator SrTiO₃ (STO) and the Mott insulator LaTiO₃ (LTO) [1]. This nearly two-dimensional metal can be easily manipulated through gate voltages and turned into a superconductor [2,3] which strikingly appears combining two nonsuperconducting materials. Superconductivity has also been observed at interfaces between two band insulators such as STO and LaAlO₃ (LAO) [4], while interfaces between different copper-based superconductors have a critical temperature higher than the bulk constituents [5,6].

The aim of this work is to develop a reliable formalism to study superconductivity in heterostructures beyond simplifying limits such as the Bardeen-Cooper-Schrieffer (BCS) approximation. In order to test the methods, we limit ourselves to s -wave superconductors with an instantaneous attraction. In order to treat superconductivity beyond any perturbative approach we use dynamical mean-field theory (DMFT) [7]. DMFT has proven successful to treat electron-electron interactions [7], electron-phonon coupling [8–11] and their interplay [12–20], as well as for the attractive Hubbard model [21–28], where the evolution of superconductivity well beyond the weak-coupling BCS regime has been studied in detail.

The extension of DMFT to treat surface and interface effects has been pioneered by Potthoff and Nolting [29,30] who introduced a layer generalization of DMFT and applied

it to a solid-vacuum interface in the presence of a short-range Coulomb interaction as described by the Hubbard model. Josephson junctions formed by superconductors and either normal or correlated metals have been studied treating the superconducting system by means of the Bogoliubov–de Gennes equations [31–34]. Including long-range Coulomb interactions Okamoto and Millis [35,36] and Kancharla and Dagotto [37] have considered charge-transfer effects and proposed that the charge leakage from one layer to another is responsible for the metallic interface between LTO and STO.

As we discuss in more detail in the following, when DMFT is extended to inhomogeneous systems, the inclusion of more and more layers is the bottleneck of the calculation. Therefore the main limitations are finite-size effects and a slow convergence to the bulk limit (infinite number of layers). Ishida and Liebsch have proposed and implemented [38,39] a strategy to overcome this limitation. The idea is to treat explicitly only a finite slab with a relatively small number of layers and to effectively describe the rest of the system with an energy-dependent embedding potential. This strategy has been shown to reduce the finite-size effects with respect to a finite slab calculation.

In this work we extend previous studied in two directions: (i) we extend the embedding potential to the superconducting state and (ii) we introduce a “feedback” effect of the slab onto the rest of the system which is shown to improve the performance of the embedding method making the finite-size effects essentially negligible already for relatively small slab sizes.

As mentioned above, the first purpose of this paper is to demonstrate the feasibility of this approach for superconducting state and to study the evolution of the physics as a function of the coupling strength. To this aim we present results for different heterostructures (solid-vacuum interface, interface between two superconductors with different coupling, interface between Mott insulator and superconductor) and we characterize the proximity effects in the three cases, showing how different observables are differently impacted by the presence of an interface. This method can be straightforwardly extended

to electron-phonon superconductors. In principle our method can also be extended to d -wave superconductors using cluster extension of DMFT. Yet we believe that our benchmarks for s -wave superconductors are precious to disentangle the effect of intermediate and strong coupling which will certainly be present for d -wave superconductors.

The paper is organized as follows. In Sec. II we introduce the model and the general concept of layered DMFT and the embedding approach. Section III is dedicated to the extension of the approach to superconducting systems and to our recipe for the embedding potential. Section IV describes our results for different physical configurations, while Sec. V contains conclusions and perspectives.

II. MODEL AND METHOD

In this section we introduce our approach to extend previous DMFT-based approaches to heterostructure to allow for superconductivity. For the sake of clarity, in the first subsection we briefly review the DMFT formalism in the superconducting state and some aspects of the exact diagonalization solution of DMFT that we employ in our practical implementation.

A. Single-site DMFT and superconductivity

Dynamical mean-field theory is one of the most popular and successful theoretical methods to treat strongly correlated electron systems. It extends the classical mean-field approach to the quantum dynamical domain by mapping a lattice model onto an effective impurity model. In the latter an interacting lattice site is hybridized with a noninteracting bath, self-consistently determined.

In this section we present the DMFT method for superconducting solutions in the specific case of the attractive Hubbard model, which can be considered the simplest model for an s -wave superconductor. However, the same equation would be found for example for an electron-phonon model or even for models without an explicit source of pairing, where superconductivity may arise from the balance between competing interactions.

The Hamiltonian reads

$$\mathcal{H} = -t \sum_{(ij)\sigma} (c_{i\sigma}^\dagger c_{j\sigma} + \text{H.c.}) - \sum_i \mu (n_{i\uparrow} + n_{i\downarrow}) - U \sum_i n_{i\uparrow} n_{i\downarrow}, \quad (1)$$

where the sums run over the sites i and j of a lattice, $c_{i\sigma}$ ($c_{i\sigma}^\dagger$) are annihilation (creator) operators for fermions with spin σ on site i , t is a nearest-neighbor hopping amplitude, U is a positive energy measuring the strength of the on-site attractive interaction, and μ is the chemical potential. This model is known to have an s -wave superconducting ground state for any value of the coupling U and it has been extensively studied by means of DMFT [21–28]. We mention that the half-filled attractive Hubbard model can be mapped exactly onto the repulsive Hubbard model. Under this transformation, the superconducting state maps onto a two-component (XY) antiferromagnetic state. Therefore our study can also be

representative of heterostructure with anisotropic (easy plane) magnetic ordering.

Within DMFT, the lattice model is mapped onto an impurity model that may be written as

$$\mathcal{H}_{\text{imp}} = \sum_{l\sigma}^{N_b} [\varepsilon_l \hat{c}_{l\sigma}^\dagger \hat{c}_{l\sigma} + (V_l \hat{c}_{l\sigma}^\dagger \hat{c}_{0\sigma} + \text{H.c.})] + \frac{\Delta_l}{2} (\hat{c}_{l\sigma} \hat{c}_{l\bar{\sigma}} + \text{H.c.}) - U \hat{n}_{0\uparrow} \hat{n}_{0\downarrow} - \mu (\hat{n}_{0\uparrow} + \hat{n}_{0\downarrow}), \quad (2)$$

where $\hat{c}_{0\sigma}^\dagger$ and $n_{0\sigma}$ are the creation and number operators of a particle with spin σ on the impurity site 0, where the interaction is present, while $\hat{c}_{l\sigma}^\dagger$ creates a particle in l th level of a noninteracting bath which is parametrized by the energy levels ε_l , the superconducting amplitudes Δ_l , and the hybridizations V_l . The amplitudes Δ_l give rise to an anomalous component of the hybridization function between the impurity and the bath which is necessary to treat the superconducting phase. The impurity model is completely characterized by the two functions

$$\mathcal{G}_{o(11)}^{-1}(i\omega_n) = i\omega_n + \mu + \sum_l |V_l|^2 \frac{i\omega_n + \varepsilon_l}{\omega_n^2 + \varepsilon_l^2 + \Delta_l^2},$$

$$\mathcal{G}_{o(12)}^{-1}(i\omega_n) = \sum_l |V_l|^2 \frac{\Delta_l}{\omega_n^2 + \varepsilon_l^2 + \Delta_l^2}, \quad (3)$$

which are the two independent component of a dynamical Weiss field.

We then see below the Green's function at the impurity site $G = -\langle T c_{0\sigma}(\tau) c_{0\sigma}^\dagger \rangle$ and its anomalous component $F = -\langle T c_{0\sigma}^\dagger(\tau) c_{0\sigma'} \rangle$ from which we build the impurity Green's function matrix in the Nambu spinor basis:

$$\hat{G} = \begin{pmatrix} G(i\omega_n) & F(i\omega_n) \\ F(i\omega_n) & -G(i\omega_n) \end{pmatrix}. \quad (4)$$

From (5) and the Weiss field matrix

$$\hat{\mathcal{G}}_o^{-1} = \begin{pmatrix} \mathcal{G}_{o(11)}^{-1}(i\omega_n) & \mathcal{G}_{o(12)}^{-1}(i\omega_n) \\ \mathcal{G}_{o(12)}^{-1}(i\omega_n) & -\mathcal{G}_{o(11)}^{-1}(i\omega_n) \end{pmatrix} \quad (5)$$

we construct the self-energy as $\hat{\Sigma} = \hat{\mathcal{G}}_o^{-1} - \hat{G}^{-1}$.

The DMFT approximation is enforced requiring that the local Green's functions [Eq. (5)] coincide with the local components of the lattice Green's function $\hat{G}_{\text{lat}}(i\omega_n) = \int d\varepsilon \rho(\varepsilon) [i\omega_n \mathbf{1}^{(2)} + (\mu - \varepsilon) \hat{\sigma}_3 - \hat{\Sigma}(i\omega_n)]^{-1}$, $\rho(\varepsilon)$ being the noninteracting density of states.

A practical implementation of DMFT requires us to recursively solve the impurity model calculating G and F . This allows us to compute the self-energy matrix and a new Weiss field $(\hat{\mathcal{G}}_o^{-1})_{\text{new}} = \hat{\Sigma} + \hat{G}_{\text{lat}}^{-1}$. The process is iterated until the Weiss fields and the other quantities are converged. In the present implementation of DMFT, we find the ground state and the Green's function of the impurity Hamiltonian using a Lanczos algorithm [40,41]. In order to obtain a finite and affordable matrix, the sums over l in Eq. (2) are truncated to a finite value N_b . The particle-hole symmetry is implemented at half-filling and the Hamiltonian is block diagonal according

to the value of S_z , while the particle number is not conserved in the superconducting state. Small values of N_b have been shown to be sufficient to obtain converged thermodynamic observables [42]. For the calculations presented in this paper we used $N_b = 7$ and we checked that results do not change increasing the number of bath sites up to $N_b = 9$. The exact diagonalization solution of DMFT involves one more step with respect to the algorithm we described. After the self-consistency condition is used to find the new Weiss field, these functions need to be cast in the form (3) with a discrete value of N_b . This can be achieved by fitting the new Weiss fields with Eq. (3) which has to be interpreted as a function of the ‘‘Anderson parameters’’ ε_l, V_l , and Δ_l . The fit procedure is performed through a conjugate gradient routine in which a distance between the new Weiss field obtained via the self-consistency and the generic form Eq. (3) is minimized as a function of the Anderson parameters. The distance can be written as

$$\chi = \sum_n^{N_{\text{MAX}}} w(i\omega_n) |(\hat{G}_o^{-1})_{\text{new}}(i\omega_n) - (\hat{G}_o^{-1})(i\omega_n)|. \quad (6)$$

Different distances can be defined by changing the number of frequencies N_{MAX} , the fictitious temperature β used to define the Matsubara frequency, and the frequency-dependent weight $w(i\omega_n)$. All the results obtained here are robust with respect to changes of the above parameters [41,42].

B. Superconducting DMFT applied to heterostructures and embedding potentials

In the previous subsections we introduced single-site DMFT for bulk superconductors, in which full translational invariance is enforced and any lattice site is equivalent. In order to study layered systems we need to use a suitable extension of DMFT able to treat inhomogeneous systems with a layered geometry. We focus on a simple cubic lattice partitioned into N layers stacked along the (001) direction. Within each layer translational invariance is assumed and the two-dimensional wave vector $\mathbf{k}_{\parallel} = (k_x, k_y)$ is a conserved quantity.

The Green’s function \hat{G}_S of a slab made of N superconducting layers can be expressed as a $2N \times 2N$ matrix corresponding to the two components of Nambu spinors and to the N layers

$$\bar{G}_S(\mathbf{k}, i\omega_n) = [(i\omega_n \mathbf{1}^{(2)} + \mu \hat{\sigma}_3) \otimes \mathbf{1}^{(N)} - \bar{\varepsilon}_{\mathbf{k}} - \bar{\Sigma}(i\omega_n)]^{-1}, \quad (7)$$

where $\mathbf{1}^{(N)}$ is the N -dimensional identity matrix and $\hat{\sigma}_3$ is the third Pauli matrix. $2N \times 2N$ matrices are identified by a bar. The single-particle dispersion matrix is given by

$$\bar{\varepsilon}_{\mathbf{k}} = \begin{pmatrix} \varepsilon_1^{\parallel} \hat{\sigma}_3 & \varepsilon_{12}^{\perp} \hat{\sigma}_3 & 0 \\ \varepsilon_{21}^{\perp} \hat{\sigma}_3 & \dots & \dots \\ 0 & \dots & \varepsilon_N^{\parallel} \hat{\sigma}_3 \end{pmatrix} \quad (8)$$

whose elements are $\varepsilon_{\alpha\alpha}^{\parallel} = -2t_{\alpha} [\cos(k_x) + \cos(k_y)]$ and $\varepsilon_{\alpha\beta}^{\perp} = t_z$. The self-energy matrix is instead a block-diagonal matrix

$$\bar{\Sigma}(i\omega_n) = \begin{pmatrix} \hat{\Sigma}_1 & 0 & 0 \\ 0 & \dots & 0 \\ 0 & 0 & \hat{\Sigma}_N \end{pmatrix}, \quad (9)$$

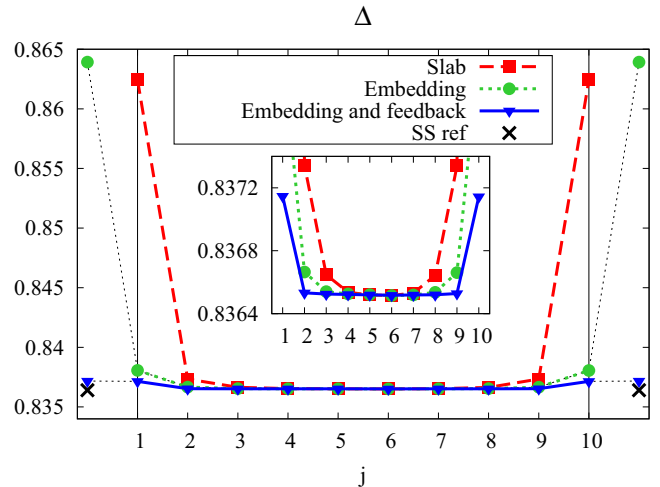


FIG. 1. Validation of our embedding scheme with feedback. We plot Δ for a ten-layer embedded system with uniform $U/t = -9$ at half-filling. The red line with squares is for the open slab, the green with dots marks the results with the embedding potential, while the blue line with triangles denotes the data corrected with the feedback of the slab. Black crosses on the two sides of the slab report the bulk DMFT result. The embedding+feedback results are essentially uniform.

where each element is a 2×2 block with normal and anomalous components corresponding to the local self-energy of an individual layer. The underlying approximation is that the self-energy remains local $\bar{\Sigma}_{ij} = \delta_{ij} \bar{\Sigma}_i$ and it is uniform within each layer, while the different layers are allowed to have different self-energies $\bar{\Sigma}_{\alpha}$, each associated with a local effective impurity problem. An explicit solution requires us to solve as many impurity models as the number of layers, from which the individual self-energies are obtained and plugged into Eq. (7). Summing over the momenta within each layer leads to a set of local Green’s functions which are then imposed to coincide with the impurity Green’s functions.

As opposed to single-site DMFT, we are therefore limited to a finite system along the z direction, which can lead to finite-size effects, that are enhanced if we use an open slab, where the electrons on the outmost layers become effectively more interacting because of the missing neighbors (Fig. 1). A possible solution to overcome this limitation is to sandwich the finite slab of N layers into two media [38,39], effectively accounting for the presence of bulk layers.

Using the notations of Ref. [43] we define the matrix inverse of (7)

$$\hat{A}_S(\mathbf{k}, i\omega_n) \hat{G}_S(\mathbf{k}, i\omega_n) = \mathbf{1}^{(2N)}. \quad (10)$$

Partitioning the infinite three-dimensional system into a slab (S) and two ‘‘bulk’’ samples (B_R and B_L) we can rewrite Eq. (10) as

$$\begin{pmatrix} \hat{A}_{B_L} & \hat{A}_{B_L 1} & 0 \\ \hat{A}_{1 B_L} & \hat{A}_S & \hat{A}_{B_R N} \\ 0 & \hat{A}_{N B_R} & \hat{A}_{B_R} \end{pmatrix} \begin{pmatrix} \hat{G}_{B_L} & \hat{G}_{B_L 1} & 0 \\ \hat{G}_{1 B_L} & \hat{G}_S & \hat{G}_{B_R N} \\ 0 & \hat{G}_{N B_R} & \hat{G}_{B_R} \end{pmatrix} = \mathbf{1}, \quad (11)$$

where the matrices are now $(2N + 4) \times (2N + 4)$. The diagonal elements of the two matrices are the Green’s functions

and the A functions for the slab (S) and the two semi-infinite substrate which embed the interacting slab. The nonzero off-diagonal elements describe the processes connecting the “left” effective substrate with layer 1 of the slab and the “right” substrate with layer N of the slab. From this we can single out the equation for the slab Green’s function

$$(\hat{A}_S - \hat{A}_{1B_L} \hat{A}_{B_L}^{-1} \hat{A}_{B_L 1} - \hat{A}_{NB_R} \hat{A}_{B_R}^{-1} \hat{A}_{B_R N}) \hat{G}_S = \mathbf{1}^{(2N)}, \quad (12)$$

which shows how the 1 and N indices are affected directly by the presence of the two semi-infinite bulks. The explicit result is

$$\hat{G}_S(\mathbf{k}, i\omega_n) = [(i\omega_n \mathbf{1}^{(2)} + \mu \hat{\sigma}_3) \otimes \mathbf{1}^{(N)} - \hat{\varepsilon}_{\mathbf{k}} - \hat{\Sigma}(i\omega_n) - \delta_{\alpha 1} \hat{S}_{B_L}(\mathbf{k}, i\omega_n) - \delta_{\alpha N} \hat{S}_{B_R}(\mathbf{k}, i\omega_n)]^{-1}, \quad (13)$$

where we have defined the complex embedding potentials

$$\hat{S}_{B_{L,R}}(\mathbf{k}, i\omega_n) = t_z^2 \hat{\sigma}_3 \hat{G}_{B_{L,R}}(\mathbf{k}, i\omega_n) \hat{\sigma}_3 \quad (14)$$

acting on the first and last layer only if the interlayer hopping is limited to nearest neighbors. Comparing with (7) it is evident that the only difference is introduced by the embedding potential at the boundaries of the slab.

C. Choice of the substrate Green’s functions

Here we introduce an optimized strategy to describe heterostructures in terms of a few “active” layers embedded between two semi-infinite systems. The starting point is naturally the surface Green’s function of a semi-infinite system. We partition a bulk system in two semi-infinite halves along the piling direction of the layers [44]. As in the rest of this work, the Green’s functions are assumed to be translational invariant along each layer and they are labeled according to the layer index. We denote the surface layer with 0 and, for the sake of definiteness, we focus on the left system with negative layer index.

The relation between the Green function of the α th layer in the left semi-infinite bulk \hat{G}_α and the same layer in the bulk crystal $\hat{G}_\alpha^{\text{bulk}}$ can be written as

$$\hat{G}_\alpha = \hat{G}_\alpha^{\text{bulk}} + \sum_{\beta} \hat{G}_\alpha^{\text{bulk}} \hat{V}_{\alpha\beta} \hat{G}_\beta, \quad (15)$$

where $V_{\alpha\beta}$ are the hopping matrix elements connecting the right and left sides with indexes $\alpha \in 0, -1, -2, \dots$ and $\beta = 1, 2, \dots$. We are only interested in the surface layer 0 which is connected only with the next layer 1 by the diagonal (in the Nambu space) hopping matrix \hat{T}_{01} , which leads to

$$\hat{G}_0 = \hat{G}_0^{\text{bulk}} (\mathbf{1}^{(2)} - \hat{G}_1^{\text{bulk}} \hat{T}_{01})^{-1}, \quad (16)$$

which requires the knowledge of the bulk Green’s function for the surface layer and for the first layer on the left, which can easily be computed within DMFT as

$$\hat{G}_\alpha^{\text{bulk}} = \int \frac{dk}{2\pi} \frac{e^{ik\alpha}}{i\omega_n \mathbf{1}^{(2)} + (\mu - \varepsilon_{\parallel} - 2t_z \cos k) \hat{\sigma}_3 - \hat{\Sigma}(i\omega_n)}, \quad (17)$$

where the Green’s function depends on the momenta along the layers \mathbf{k}_{\parallel} while the integral on the left-hand side is performed

over the transverse momentum. The self-energy in Eq. (17) is determined self-consistently solving two more impurity models coupled with the slab. The \hat{G}_0 in Eq. (16) defines the left embedding potential in Eq. (13). The right potential is obviously identical.

D. Observables

To characterize the superconducting states of our layered superconductor and its spatial dependence we focused on a few relevant observables. The most direct evidence of the superconducting state and its strength is the layer-resolved zero-temperature pairing amplitude, simply obtained as the integral of the anomalous part of the α th layer Green’s function

$$\Delta_\alpha = T \sum_n F_\alpha(i\omega_n) = \langle c_{\alpha\uparrow}^\dagger c_{\alpha\downarrow}^\dagger \rangle. \quad (18)$$

Which indeed correspond to the equal-time pair amplitude. The nature of the superconducting state (for example if the system is in an effective weak- or strong-coupling regime) can be characterized in terms of the different contribution to the total energy. The layer-resolved potential energy is simply

$$E_{\text{pot}}^\alpha = U \langle \hat{n}_{o\uparrow} \hat{n}_{o\downarrow} \rangle_\alpha, \quad (19)$$

while the kinetic energy reads

$$\langle E_k^\alpha \rangle = T \sum_n \int d\epsilon \rho(\epsilon) \text{Tr} \{ \epsilon \hat{\sigma}_3 \hat{G}_\alpha(\epsilon, i\omega_n) \}. \quad (20)$$

Notice that while the global order parameter and potential energy are simply obtained by summing the contributions from the different layers, the bulk kinetic energy also includes the contributions from the interlayer hoppings, which do not contribute to the above $\langle E_k \rangle$. Finally we can compute the quasiparticle weight, namely $z_\alpha = [1 - \partial \Sigma_\alpha^{11}(i\omega_n) / \partial (i\omega_n)|_{i\omega_n \rightarrow 0}]^{-1}$. Where $\Sigma_\alpha^{11}(i\omega_n)$ is the normal component of the α th layer self-energy. We use z_α as a measure of the coherence of the low-lying excitations at the gap edge. In a BCS superconductor these excitations are completely coherent and we recover $z = 1$, while increasing the coupling it decreases even if slightly.

E. Benchmark for homogeneous systems

Figure 1 presents results for a ten-layer slab for uniform parameters $U/t = -9$ and half-filling. In the absence of any embedding potential, the slab breaks translational symmetry and the order parameter Δ becomes larger at the edges. Introducing the embedding potential according to the described scheme, we obtain the results shown as a dotted green line with large dots in Fig. 1. Here we consider completely uniform interaction strength, and noticed that the embedding potentials strongly reduces the inhomogeneity, even if a minor enhancement of the order parameter is clear at the edges of the slab.

In order to further reduce the effects of the finiteness of the slab, in this work we propose a simple strategy to improve the scheme, introducing a *feedback* of the slab on the semi-infinite bulks. The idea is simply to define a potential created by the slab onto the semi-infinite bulks on the two edges. This is simply realized by adding a potential term similar to Eq. (14)

to the self-energy of each semi-infinite systems

$$\hat{S}_{FB,L,R}(\mathbf{k}, i\omega_n) = t_z^2 \hat{\sigma}_3 \hat{G}_{S_{1,N}}(\mathbf{k}, i\omega_n) \hat{\sigma}_3. \quad (21)$$

The data in Fig. 1 demonstrate that the feedback further reduces the inhomogeneity and it allows us to essentially reproduce the uniform bulk even with a very limited number of layers.

In Fig. 2 we demonstrate that our feedback performs accurately for different observables and for any value of the parameters. We consider again homogeneous parameters and we vary the value of the interaction U . Here we plot the average over the slab of Δ , Z , and of the double occupancy D as a function of U and we compare with a bulk cubic lattice (which should be reproduced when the finite-slab effect are canceled) and, for reference with a two-dimensional calculation corresponding to a single layer. To illustrate the general validity of our approach we consider both a negative U , for which we find superconductivity, and a positive U model, in which s -wave superconductivity cannot establish and therefore represents the normal state. The three panels of Fig. 2 clearly show that for every value of U the three observables coincide with their bulk counterparts.

III. RESULTS

In this section we present some results using the embedding+feedback procedure for an attractive Hubbard model. In this work we limit ourselves to paradigmatic situations and we postpone to future applications more realistic setups corresponding to actual materials and heterostructure. We fix the local density to one electron per site on each layer by imposing particle-hole symmetry. This obviously freezes charge redistribution across the interface. We chose to start with this situation to single out the intrinsic effects due to the proximity from the effects due to charge transfer across the interface, which would obviously affect the results. Interestingly, we find important proximity effect even in this case.

A. Weak/strong interacting superconductor

As a first example we consider the interface between two semi-infinite systems with different values of the attractive interaction, considering ten active layers for both systems. In Fig. 3 we present results in which we fix the interaction at a relatively small interaction $U/t = -3$ on the left side, while on the right side we tune the interaction from $U/t = -3$ to a much larger attraction $U/t = -7.5$. We present layer-resolved pairing amplitude Δ_α , quasiparticle weight z_α , double occupancy D_α , and in-plane kinetic energy $\langle E_{k\alpha} \rangle$ as a function of the layer index α . On the right side of the figure the bulk values are shown for reference.

We first observe that also in this case our embedding+feedback scheme provides an essentially continuous connection between the leads (corrected by the feedback) and the first layers which we explicitly treat with layered DMFT. The evolution across the slab is rather smooth, especially for the order parameter, shown in Fig. 3(a), for which a significant proximity effect leads to an enhancement of the order parameter on the left side which penetrates for almost ten layers. The effect is quantitatively significant.

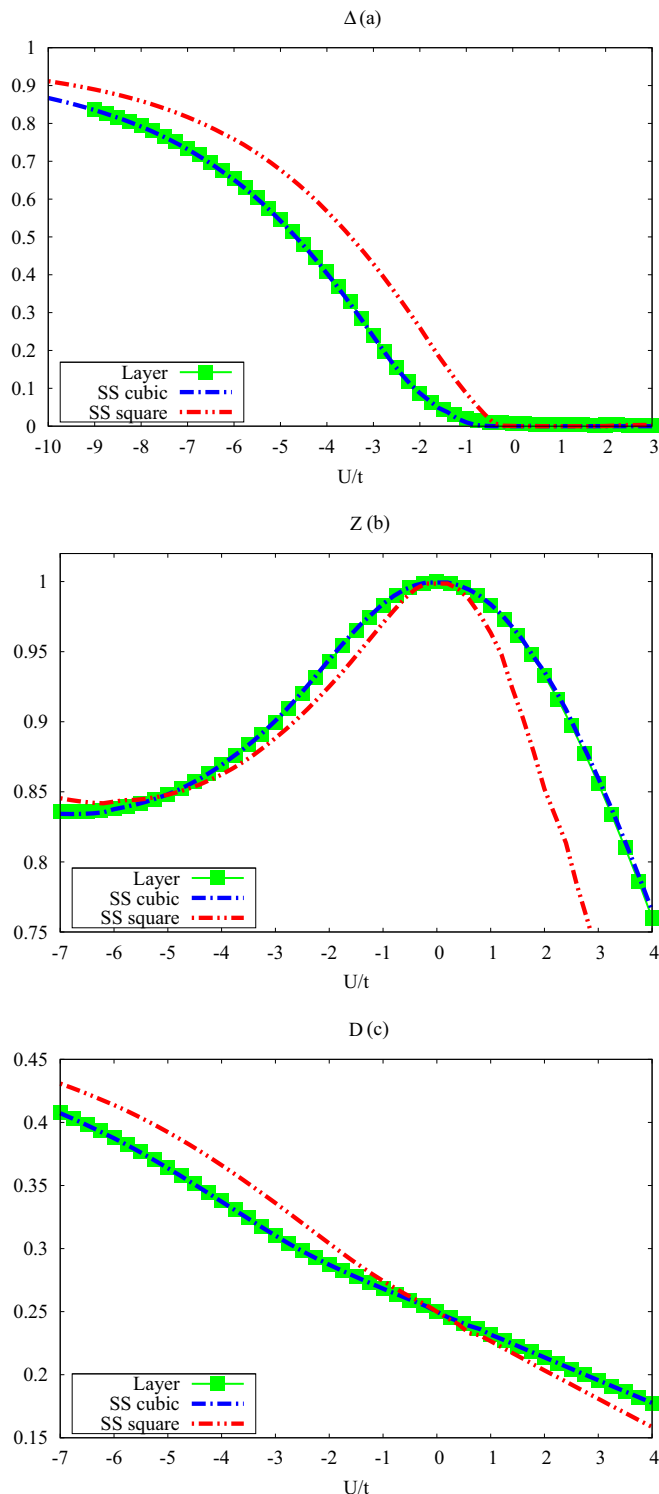


FIG. 2. (a) Order parameter Δ , (b) quasiparticle weight z , and (c) double occupations expectation value $D = \langle \hat{n}_{o\uparrow} \hat{n}_{o\downarrow} \rangle$ vs interaction strength U at half-filling. Red and blue lines refers, respectively, to the square and cubic lattice, single site DMFT calculations. Green dots represents the results for the central plane of an homogeneous system made of seven layers, similar to the blue one in Fig. 1.

For example the order parameter in the first layer of the weak-coupling superconductor can be increased by 50% when the pairing amplitude of the right system is $U = -7t$.

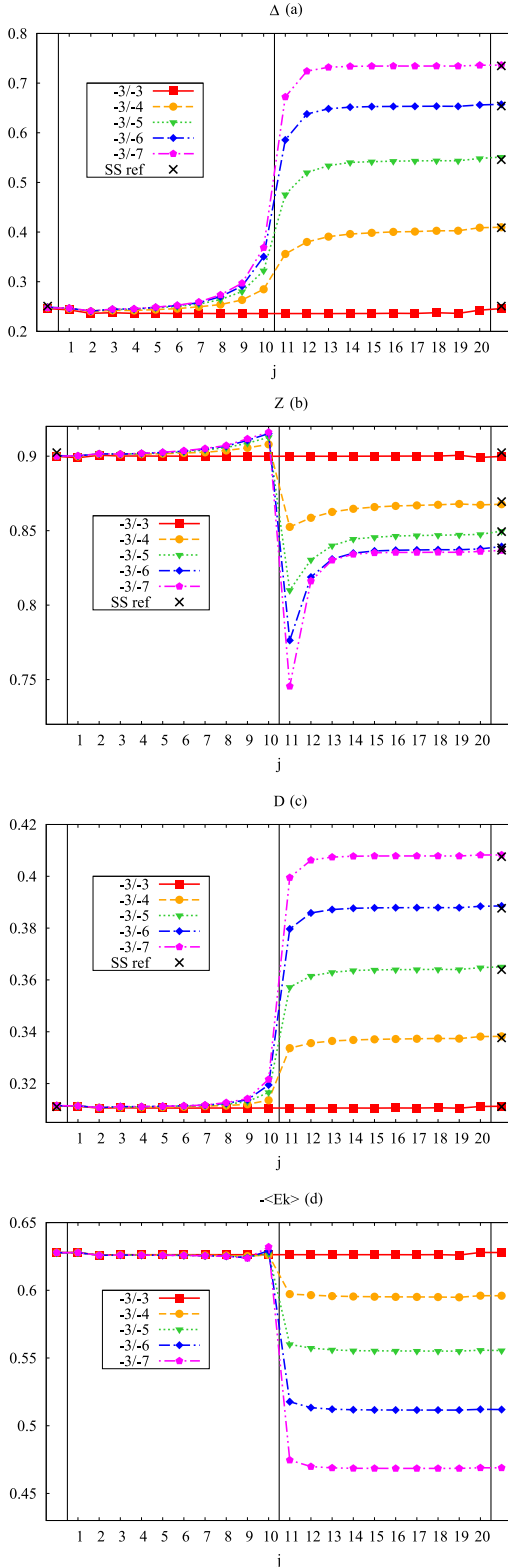


FIG. 3. $\Delta_\alpha, z_\alpha, D_\alpha,$ and $-\langle E_k \rangle$ in a 20-layer thick heterostructure formed by two semi-infinite halves. The left half (index ≤ 10) is kept at $U/t = -3$, while for the right half (index ≥ 11) we used different values of the attraction with equal or larger absolute value. The points outside the heterostructure are those computed starting from the leads' Green's functions used to compute the embedding potential \hat{G}_B . The crosses are the results for a bulk DMFT calculation for the cubic lattice.

Also the right side is substantially affected by the presence of the weakly coupled superconductor. The reverse effect on the strong-coupling superconductor is however smaller in absolute and relative terms with an order parameter which is reduced at most of 10%. Interestingly the spatial extent over which the order parameter is not strongly dependent on the value of the interaction in the right half. The double occupancy, which is also related to the potential energy has a similar evolution, but the proximity effects are limited to a thinner slice of the slab of around three layers and the relative change induced by proximity is much smaller. A similar behavior is shown by the layer kinetic energy, which is negative and larger in amplitude on the left (weak-coupling side). Interestingly, the presence of the stronger-coupling superconductors leads to a slight increase of the modulus of the kinetic energy in the first layers of the weak-coupling side. Finally, the quasiparticle weight, which can be used to measure the coherence of the electronic excitations, is slightly increased in the weak coupling side, and it decreases in the strong-coupling region, even if all these variations are relatively small.

In Fig. 4 we present an analogous analysis in which the left side has a constant $U/t = -10$ while on the right side the interaction goes from $-10t$ to $-3t$. The qualitative results are similar to the previous even if the proximity effects are reduced both in their spatial extension and in the strength of the effect because of the stronger coupling on the left side, which leads to a short coherence length and the physics becomes more local. Still, a clear intermediate region, where the physical quantities smoothly connect, appears. Also in this case, the effect is quantitatively stronger for the superconducting order parameter, which is again increased up to a factor 2 on the weaker-coupling side (now the right half).

B. Correlated metal/superconductor

We now move to a different situation where one of the two halves of the system would not be superconducting by itself. On the left side we consider a metal with a finite repulsion $U/t = 4$, which would lead to a moderately correlated metal in a bulk system, while on the right we tune the attractive interaction from 0 to $U = -6t$. The results, plotted in Fig. 5, show that despite the repulsive interaction superconductivity can penetrate for a few layers of the metal, and that important effects are observed on the superconducting side. This is a clear qualitative violation of the local-density approximation even in the absence of charge redistribution across the interface. The effect on the order parameter is small but clearly visible (one obtains an order parameter which is around 0.05 the bulk value on the superconducting side), while the double occupancy is essentially unaffected by the connection between the two semi-infinite systems. The kinetic energy presents an interesting increase (in modulus) in the first layers of the metallic system, the same region where superconductivity is able to penetrate in the repulsive metal.

These results clearly demonstrate that the approach we have devised is able on one hand to reproduce the bulk results when we are sufficiently far from the interface and on the other hand to display nontrivial and interaction dependent proximity effects, which can lead to important effects in real systems. The

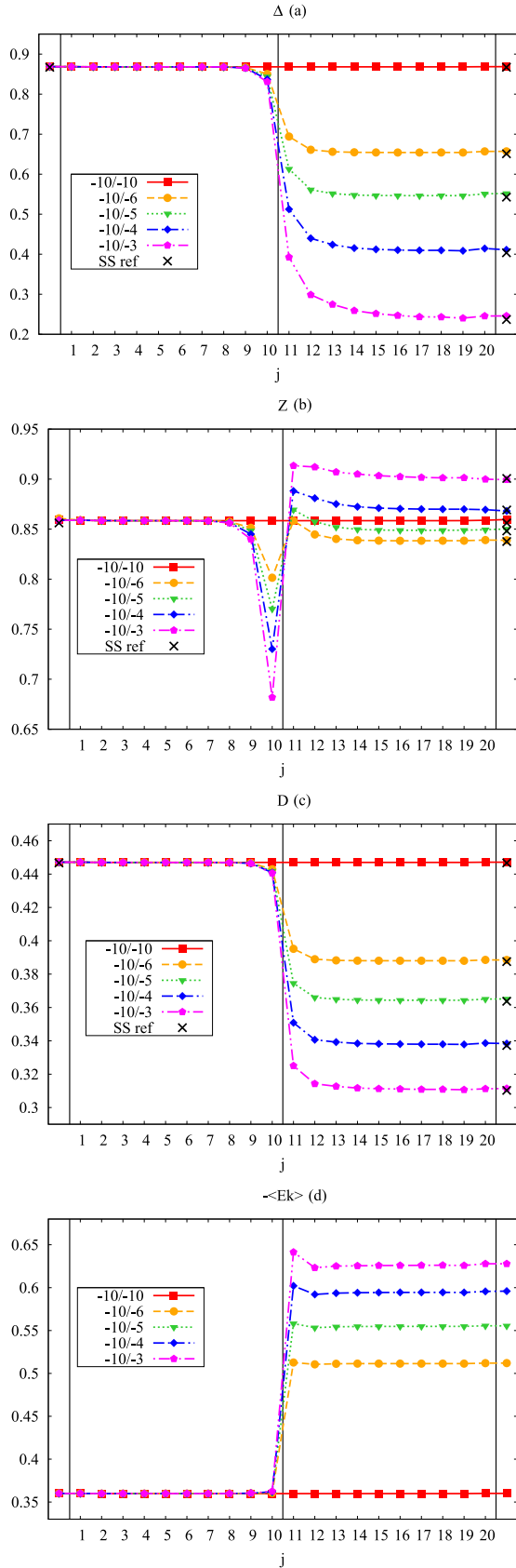


FIG. 4. $\Delta_\alpha, z_\alpha, D_\alpha,$ and $-\langle E_k \rangle$ in a 20-layer thick heterostructure. The left half (index ≤ 10) is kept at $U/t = -10$, while for the right half (index ≥ 11) we used smaller or equal values of the attraction strength.

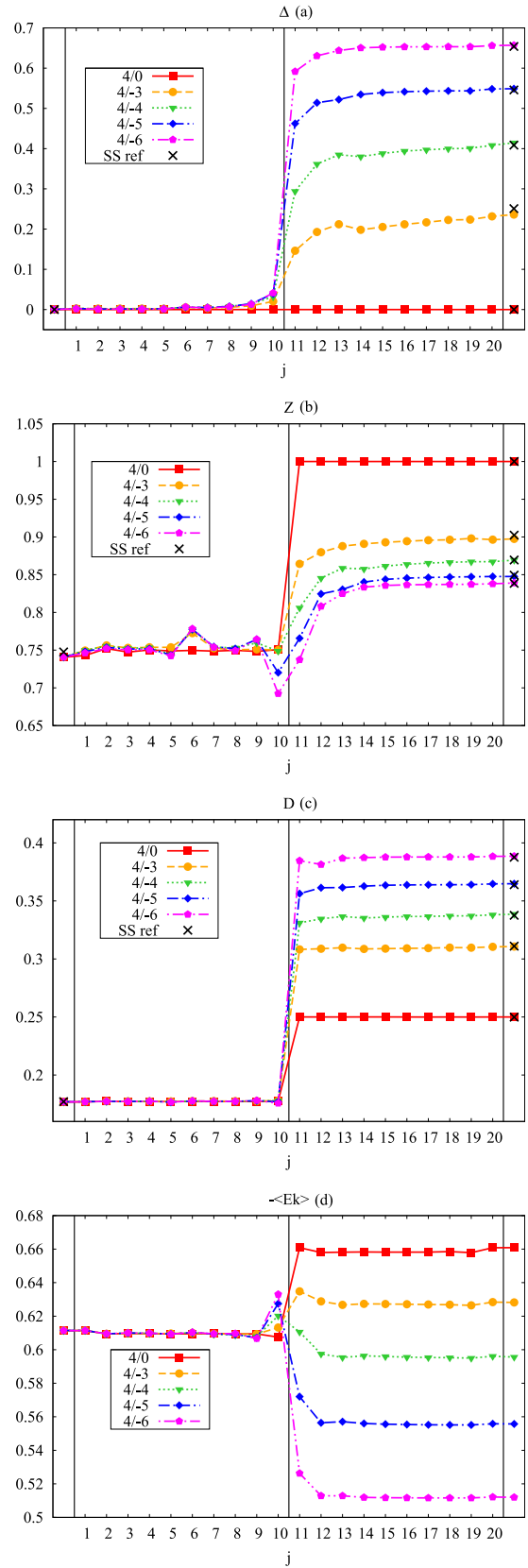


FIG. 5. $\Delta_\alpha, z_\alpha, D_\alpha,$ and $-\langle E_k \rangle$ in a 20-layer thick heterostructure. Here on the left side we have a correlate metal with a repulsive $U/t = 4$, while on the right side we tune an attractive interaction. The wiggles in the quasiparticle weight are a numerical artifact due to the small energy scales involved in the calculation of the derivative.

effect is generally stronger for the order parameter than for the other observables we considered.

IV. CONCLUSION

In the present work we have introduced an effective extension of the embedding approach which allows us to study heterostructure of interacting systems by means of a small number of active layers. Our extension is twofold. We extend the formalism to the superconducting state, and we also introduce a “feedback” of the slab onto the embedding potential which reduces the finite-size effects introduced by the finiteness of the slab. We have demonstrated that the feedback correction indeed dramatically reduces the effects of a finite slab and it produces essentially exact results for all the relevant layer-resolved observables when treating homogeneous bulk systems.

After having established the accuracy of the refined embedding approach, we have also presented two applications of the method to paradigmatic situations where a heterostructure is formed out of two semi-infinite systems separated by a two-dimensional interface. In particular, we consider a superconductor with different values of the attractive strength connected with either a superconductor or a metal with intermediate repulsive interactions. We find that in the first case important proximity effects take place and stronger superconductor increases the superconducting order parameter for around ten layers for a wide range of parameters. In the second case superconductivity penetrates in the repulsive system for around two layers, qualitatively changing the physics of the system. In both cases the strongest effects are seen on the order parameters, while the kinetic and potential energies remain closer to the results for two disconnected systems. It is worth mentioning that, imposing particle-hole symmetry and fixing every layer to be half-filled, we freeze

the charge redistribution which would naturally enhance the effects we describe.

In this paper we limited to the simple attractive Hubbard model at half-filling in order to benchmark our method and, more importantly, to single out the effects associated with the strength of the coupling from the variety of effects happening at a real interface. Indeed our results demonstrate that this approach can be used to study interface or heterostructures involving two superconductors with different coupling strength, which can be seen as a greatly simplified version of heterostructures involving copper oxides with different doping, or heterostructures involving Mott insulators and s -wave superconductors. However, our method can be extended to include several realistic features. For example, the approach can be applied to the paradigmatic LTO/STO system, where the STO can be modeled as a Mott insulator with positive U , while LTO can be described as a band insulator with a weak electron-phonon interaction. The latter can be either approximated with an attractive Hubbard interaction or with an actual coupling between the electrons and phononic degrees of freedom. Indeed our approach can be straightforwardly extended to models in which the s -wave superconductivity arises from electron-phonon coupling of the Holstein type. In this case one could study if the presence of STO can turn LTO into a superconductor by providing carriers to the band insulator, thereby activating the BCS pairing as in doped bulk LTO. Furthermore, the present approach can also be combined with density-functional theory to introduce the realistic electronic structure and close the gap with actual materials.

ACKNOWLEDGMENTS

We thank A. Amaricci and G. Giovannetti for useful discussion. This work has been supported by the European Union under FP7 ERC Starting Grant No. 240524 “SUPERBAD.”

-
- [1] A. Ohtomo, D. A. Muller, J. L. Grazul, and H. Hwang, *Nature (London)* **419**, 378 (2002).
 - [2] J. Biscaras, N. Bergeal, A. Kushwaha, T. Wolf, A. Rastogi, R. Budhani, and J. Lesueur, *Nat. Commun.* **1**, 89 (2010).
 - [3] J. Biscaras, N. Bergeal, S. Hurand, C. Grossetête, A. Rastogi, R. C. Budhani, D. LeBoeuf, C. Proust, and J. Lesueur, *Phys. Rev. Lett.* **108**, 247004 (2012).
 - [4] N. Reyren, S. Thiel, A. D. Caviglia, L. F. Kourkoutis, G. Hammerl, C. Richter, C. W. Schneider, T. Kopp, A.-S. Rüetschi, D. Jaccard, M. Gabay, D. A. Muller, J.-M. Triscone, and J. Mannhart, *Science* **317**, 1196 (2007).
 - [5] H. Hwang, Y. Iwasa, M. Kawasaki, B. Keimer, N. Nagaosa, and Y. Tokura, *Nat. Mater.* **11**, 103 (2012).
 - [6] J. Chakhalian, J. W. Freeland, A. J. Millis, C. Panagopoulos, and J. M. Rondinelli, *Rev. Mod. Phys.* **86**, 1189 (2014).
 - [7] A. Georges, G. Kotliar, W. Krauth, and M. J. Rozenberg, *Rev. Mod. Phys.* **68**, 13 (1996).
 - [8] J. K. Freericks, M. Jarrell, and D. J. Scalapino, *Phys. Rev. B* **48**, 6302 (1993).
 - [9] A. J. Millis, R. Mueller, and B. I. Shraiman, *Phys. Rev. B* **54**, 5389 (1996).
 - [10] D. Meyer, A. C. Hewson, and R. Bulla, *Phys. Rev. Lett.* **89**, 196401 (2002).
 - [11] M. Capone and S. Ciuchi, *Phys. Rev. Lett.* **91**, 186405 (2003).
 - [12] J. K. Freericks and M. Jarrell, *Phys. Rev. Lett.* **75**, 2570 (1995).
 - [13] A. Deppeler and A. J. Millis, *Phys. Rev. B* **65**, 100301 (2002).
 - [14] W. Koller, D. Meyer, and A. C. Hewson, *Phys. Rev. B* **70**, 155103 (2004).
 - [15] G. Sangiovanni, M. Capone, C. Castellani, and M. Grilli, *Phys. Rev. Lett.* **94**, 026401 (2005).
 - [16] P. Werner and A. J. Millis, *Phys. Rev. Lett.* **99**, 146404 (2007).
 - [17] G. Sangiovanni, M. Capone, and C. Castellani, *Phys. Rev. B* **73**, 165123 (2006).
 - [18] M. Capone, C. Castellani, and M. Grilli, *Adv. Condens. Matter Phys.* **2010**, 920860 (2010).
 - [19] G. Giovannetti, M. Casula, P. Werner, F. Mauri, and M. Capone, *Phys. Rev. B* **90**, 115435 (2014).
 - [20] Y. Nomura, S. Sakai, M. Capone, and R. Arita, *Sci. Adv.* **1**, e1500568 (2015).

- [21] M. Keller, W. Metzner, and U. Schollwöck, *Phys. Rev. Lett.* **86**, 4612 (2001).
- [22] M. Capone, C. Castellani, and M. Grilli, *Phys. Rev. Lett.* **88**, 126403 (2002).
- [23] A. Toschi, M. Capone, and C. Castellani, *Phys. Rev. B* **72**, 235118 (2005).
- [24] A. Toschi, P. Barone, M. Capone, and C. Castellani, *New J. Phys.* **7**, 7 (2005).
- [25] A. Garg, H. R. Krishnamurthy, and M. Randeria, *Phys. Rev. B* **72**, 024517 (2005).
- [26] J. Bauer and A. C. Hewson, *Europhys. Lett.* **85**, 27001 (2009).
- [27] J. Bauer, A. C. Hewson, and N. Dupuis, *Phys. Rev. B* **79**, 214518 (2009).
- [28] A. Koga and P. Werner, *Phys. Rev. A* **84**, 023638 (2011).
- [29] M. Potthoff and W. Nolting, *Phys. Rev. B* **59**, 2549 (1999).
- [30] M. Potthoff and W. Nolting, *Phys. Rev. B* **60**, 7834 (1999).
- [31] P. Miller and J. K. Freericks, *J. Phys. Condens. Matter* **13**, 3187 (2001).
- [32] J. K. Freericks, B. K. Nikolić, and P. Miller, *Phys. Rev. B* **64**, 054511 (2001).
- [33] B. K. Nikolić, J. K. Freericks, and P. Miller, *Phys. Rev. Lett.* **88**, 077002 (2002).
- [34] A. N. Tahvildar-Zadeh, J. K. Freericks, and B. K. Nikolić, *Phys. Rev. B* **73**, 184515 (2006).
- [35] S. Okamoto and A. J. Millis, *Phys. Rev. B* **70**, 241104 (2004).
- [36] S. Okamoto and A. J. Millis, *Phys. Rev. B* **70**, 075101 (2004).
- [37] S. S. Kancharla and E. Dagotto, *Phys. Rev. B* **74**, 195427 (2006).
- [38] H. Ishida and A. Liebsch, *Phys. Rev. B* **79**, 045130 (2009).
- [39] H. Ishida and A. Liebsch, *Phys. Rev. B* **82**, 045107 (2010).
- [40] M. Caffarel and W. Krauth, *Phys. Rev. Lett.* **72**, 1545 (1994).
- [41] M. Capone, L. de' Medici, and A. Georges, *Phys. Rev. B* **76**, 245116 (2007).
- [42] A. Liebsch and H. Ishida, *J. Phys. Condens. Matter* **24**, 053201 (2012).
- [43] R. Nourafkan, M. Capone, and N. Nafari, *Phys. Rev. B* **80**, 155130 (2009).
- [44] D. Kalkenstein and P. Soven, *Surf. Sci.* **26**, 85 (1971).